Paper

An Efficient Model for Inspecting the Quality of Pellet Components Automatically

Non-member	Ningfeng ZENG	(Fukui University)
Non-member	Hiroshi YAMAMOTO	(SYSMEX Corp.)
Non-member	Toshihiro KONAKA	(SYSMEX Corp.)
Member	Keiji TANIGUCHI	(Fukui University)

This paper proposes an efficient method based on neural networks to automatically determine the quality of pellet components. By using two images (front and side views, referred to below as CIFV and CISV respectively) captured through the microscope using a CCD camera, it is possible to assess the quality of pellet component. Here we define the captured image in front view as CIFV and the captured image in side view as CISV. In addition, Two corresponding template images are defined here as TIFV for front view and TISV for side view, respectively. These template images were created based on the design dimension. Prior to carrying out the quality evaluation, the captured images were processed to eliminate noise and the images were binarized. Then, the datum matching plane and the datum machining line for the captured images were calculated. Next, using a coordinate transformation related to the positions of the datum plane and the datum line, the test hole in the captured image can be moved to the center part of this image in order to match the template image. After that, the values of certain feature parameters are calculated based on the errors and on the differences between the captured images and template images. Finally, the values of parameter features serve as inputs of the neural networks for determining the quality of the component. The experimental results confirm the effectiveness and efficiency of this procedure for inspecting the quality of pellet components.

Keywords : Quality Inspection, Template Image, Template Matching, Back-Propagation Neural Networks, Pellet Component, Similarity

1. Introduction

The pellet component which is made of ruby is used in blood analysis system which is usually called Automated Hematology Analyzer[1][2] . In the center of this component, there is a hole (an orifice) in which blood passes through. This hole is the most important part for counting the number of blood cells in blood analysis system. The accuracy of the hole machining in the component contributes to good performance of the blood analysis system. In this paper, we propose a method for testing the quality of this hole of the component by using neural networks, and inspecting the quality based on the global properties of component rather than each data of the component dimensions[3][4].

2. The previous work and its problem

The measurement system is composed of a microscope, a CCD camera, a personal computer, X-Y stager & Micro Scanner[5] and an auto- focusing device[6] which are connected with the microscope. The software of this system is Microsoft Visual C++ Version 5.0 Professional Edition. This system of the hardware is shown in Fig.1.

In ref. (3), the method now has been able to measure the dimensions of the important part of the component, and also has been able to fill the dimensions in statistical table automatically. Therefore, this method is able to save on time to measure the dimensions and have higher precision than previous manual method. However, there are still some problems: the error rises from the measured positions located by using the differential method[3], and the determination of quality is not precise. The traditional methods[3][7][8][9][10] evaluate the quality of a component by using linear determination for each value or the combination of several linear decisions. Therefore, these methods are difficult to determine some complex cases.

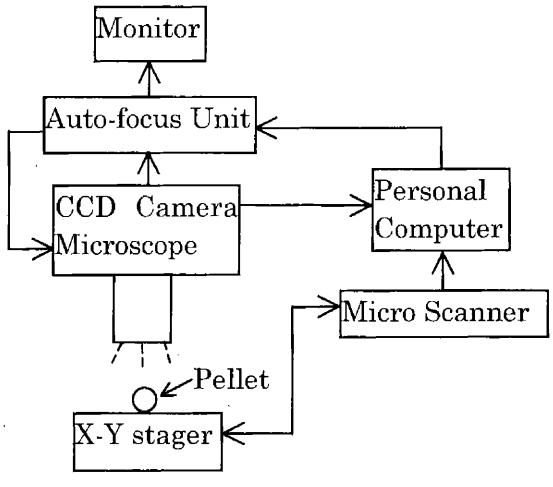

Fig.1 Dimension measurement system for the pellet component

In order to decrease the errors after auto-calibration and auto-focusing, the positions in the X-Y stager and the focus stager are adjusted slightly until the optimum image could be captured for the measurement. On the other hand, we

use the template image and template match to decrease the errors which are described above. In this paper, the quality evaluation do not base on the large sum of data, but base on the global properties of the pellet component. We not only take the advantage of precise calculation of computer and also try to employ the artificial intelligence to make the determination.

3. Image Analysis

3.1 Template image Figs.2(a) shows the dimensions of the pellet component in front and side views, respectively. The diameter of this component is 6mm and the thickness is 0.4 mm. Here, we only concern the hole in the center part, in which the internal diameter of this hole is only 0.1mm and the thickness of the center part is only 0.12 mm. Figs.2(b) and (c) illustrate the template images in the side and front views, respectively. By using C language, both of them were created based on the design dimensions. In this paper, the image shown in Fig.2(c) is defined as a Template Image in Front View (TIFV). In the meantime, the image shown in Fig.2(b) is defined as a Template Image in Side View (TISV).

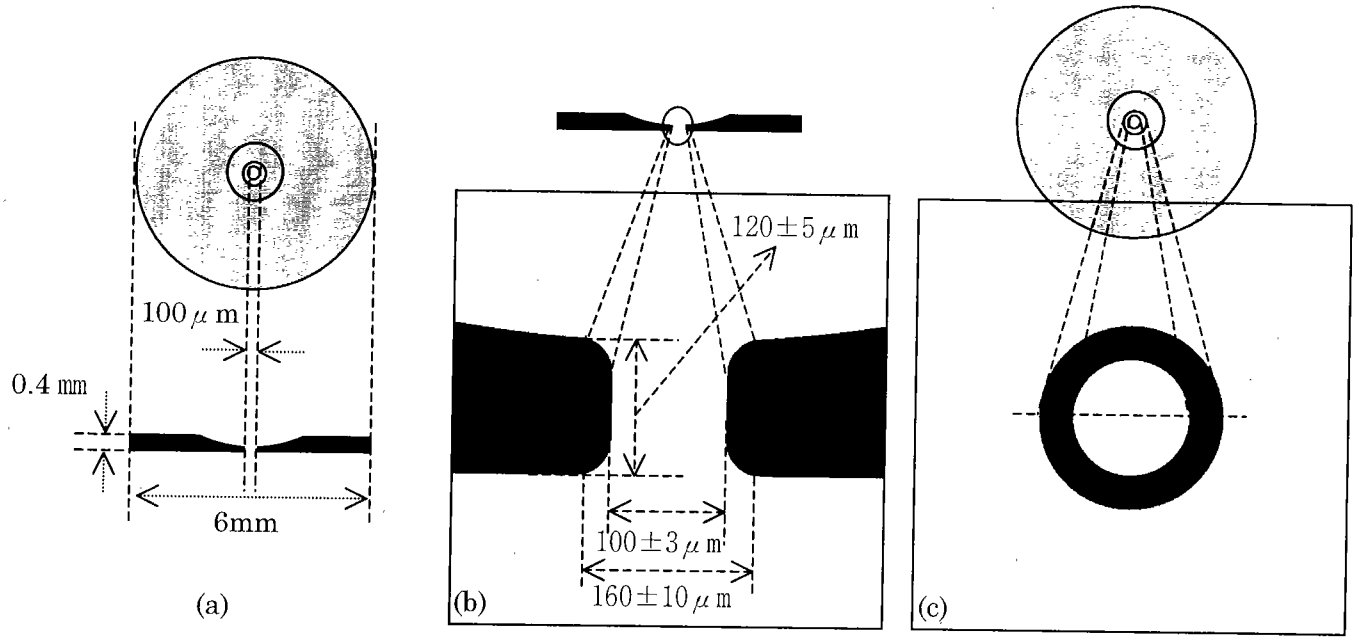

Fig.2 Pellet component and its template images, (a) the component in front and side views, (b) the pellet component in side view and its template image (TISV), (c) the component in front view and its template image (TIFV)

3.2 Captured image and its processing

3.2.1 The image in side view and its processing

Fig.3 shows an original color image (CISV) which was captured by CCD camera after auto-focusing of the microscope and calibration of the position.

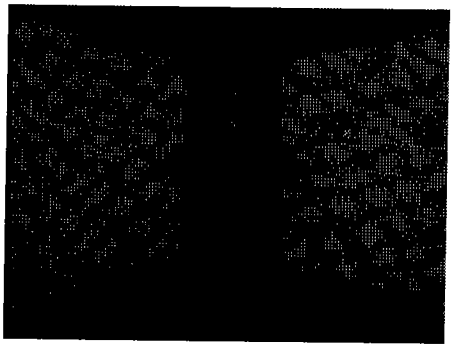

Fig.3 The original image (CISV) in the side view

In order to improve the efficiency for the processing, the image was decomposed into RGB primaries. From them we selected the R primary which is shown in Fig.4(a), because the red primary represents the most information of the original color image. In this image, the object can be discriminated from the background easily. Therefore, the image can be binarized by using single threshold value. The binarized result was shown in Fig.4(b). In Fig.4(a), there is a dotted line. The upper side of the line is the real image and the lower side of the line is the virtual image. Usually the real image is used to process here. Therefore the position of dotted line which is datum of the machining plane have to be calculated. Fig.4(c) shows the object boundary which is detected from the binarized image by using the difference of its intensities. Based on this boundary image, the two datum lines which are shown in Fig.4(d) were calculated. First, the point (a, b) of the cross between the real and the virtual parts shown in Fig.4(c) is located according to the shape change of the edge. Based on the two points, we can draw line(1). Second, the algorithm for obtaining line (2) is shown as follows:

$$line(i) = (ed_1(i) + ed_2(i))/2 \qquad (1)$$

where $ed_1(i)$, $ed_2(i)$ are horizontal coordinates of the left and right edges, i is the vertical coordinate. Then, the coordinates of the line is gotten, the line sometime might be a curve but not straight line. Therefore, the least square estimate is used to calculate a straight line which is shown

as line (2). By combining the datum line(1) shown in Fig.4(d), the real image shown in Fig.4(e) was able to be gotten from the binarized image shown in Fig.4(b). In the final step, based on the position of both of the datum lines (1) and (2), the tested object can be moved to the center of the image which is shown in Fig.4(f).

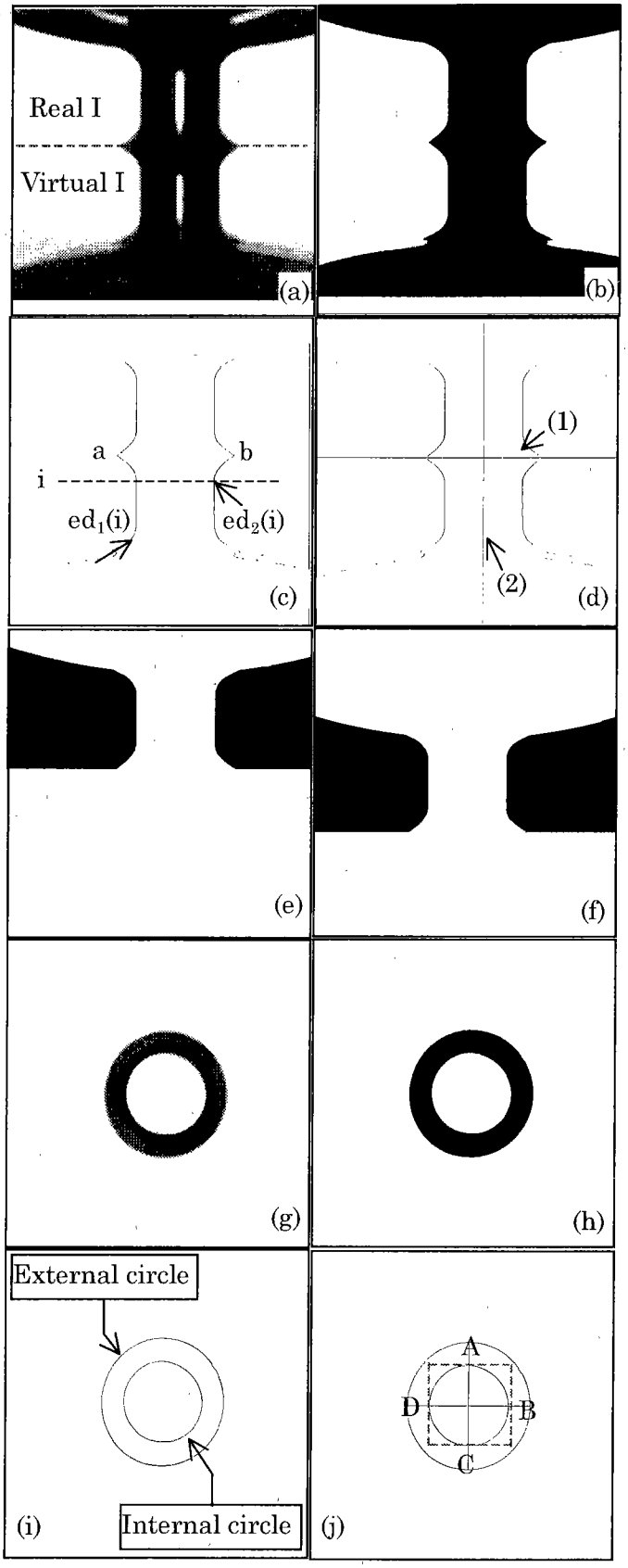

Fig. 4 The captured images and its processing, (a)-(f) The processing for captured image in the side view, (g)-(j) The processing for captured image in the front view.

3.2.2 The image in front view and its processing Figs. 4(g-j) show the processing of the captured image in front view (CIFV) of the pellet component. Fig.4(g) shows the red primary of an original color image in front view. Fig.4(h) is a binarized image of Fig.4(g). By using the difference of the gray level value, the boundary image shown in Fig.4(i) was obtained from Fig.4(h). Then, by using the scanning method, the coordinates of intersections (A,B,C,D) between the dotted lines and the circle shown in Fig.4(j) are able to be calculated. Fig.4(k) also shows the method for calculating center point in detail. Based on the coordinates of the four points(A,B,C,D) on the circle, the coordinate of the center point in the circle is able to be calculated. According to the machining methods and experimental data, usually, the round shape might not change rapidly. Therefore, we use a square to match the outline of the measured object. Next, the coordinate(I_1,J_1,I_2,J_2) of the square shown in Fig.4(k) can be obtained. Then, the coordinate of the circle center (x,y) is calculated by the following equation:

$$x=(I_1+I_2)/2; \quad y=(J_1+J_2)/2$$

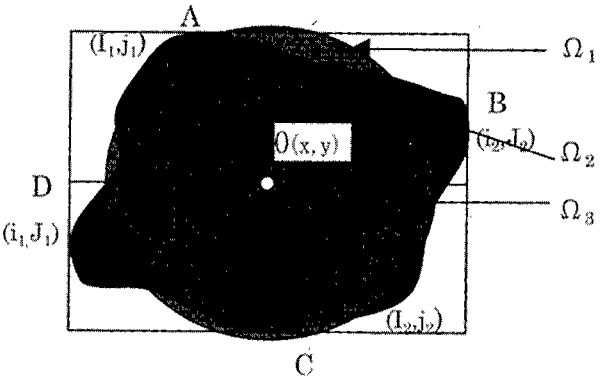

Fig.4(k) The error of measured circle is enlarged.

Finally, in order to match for the template image, the whole circle ring was moved to the central part of the image, based on the coordinate of the center point of the external and internal circles respectively.

4. Image matching and the quality analysis

4.1 Image matching According to machining methods of the component, usually, several possible problems of the errors which deteriorate the quality of the pellet component could occur. Therefore, our method here is concerned mostly for these possible problems to evaluate the quality of the pellet component. In the front view, as shown in Fig.4(k), the features of quality are the error sizes of both the internal and the external circles, the circularity of both the internal and the external circles which are edge of Fig.4(g) shown in Fig.4(i), the eccentricity between the internal and the external circles.

Those parameters are defined as features for the evaluation of the quality of the component. On the other hand, in the side view, as shown in Fig.5(a), the important parameters are the similarity between the template and the captured images, the size of different(error size) between the template and the captured images, the verticality of the hole in the middle part and the symmetry between the left and the right parts in the image. In Ref. (9)-(13), there are many methods to calculate the circularity and the similarity. Here we propose a more simple method to calculate them and to evaluate the quality.

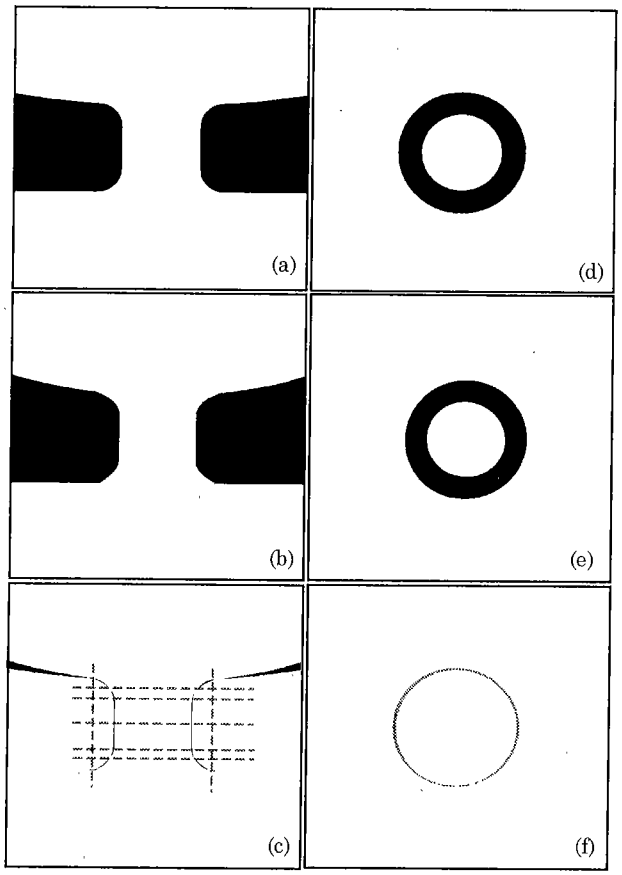

Fig.5 Image matching between the template and the captured images. (a) The template image of component in the side view(TISV), (b) the final result obtained from CISV, (c) the matching result of side view between (a) and (b), (d) the template image in front view(TIFV), (e) the final result gotten from CIFV, (f) the matching result of the front view between (d) and (e).

Fig.5 shows the image matching between the template and the captured images. Fig.5(c) shows the matching result between the template image Fig.5(a) and captured image Fig.5(b). In the same way, Fig.5(f) is the matching result between Fig.5(d) and (e). A value a_1 (e.g. 150) is used to represent the gray level of the object for Figs.5(a) and (d), in the meantime , another value a_2 (e.g. 250) is used to represent that for Figs.5(b) and (e). Then, the result M(i,j) can be obtained as follows:

$$M(i,j)=|T(i,j)-C(i,j)| \quad \cdots\cdots (1)$$

where T(i,j) and C(i,j) denote the intensities of the template and the captured images, respectively. The image M(i,j) is used to calculate the errors. An example is shown in Fig.4(k) that the error was enlarged. In this figure, Ω_1 represents the area of the different part inside the template circle, Ω_2 represents the area of the different part outside the template circle and Ω_3 represents overlapped part.

4.2 Feature parameters The feature parameters are calculated based on matching results in front and side views shown in Figs.5(c) and (f), respectively.

4.2.1 Feature parameters for the front view In front view, the following problems of errors are considered: both of the circularity(roundness) of the internal and the external circles, the errors of size differences between the template and the captured images, both of the symmetries of internal and external circles, the eccentricity between the internal and the external circles.

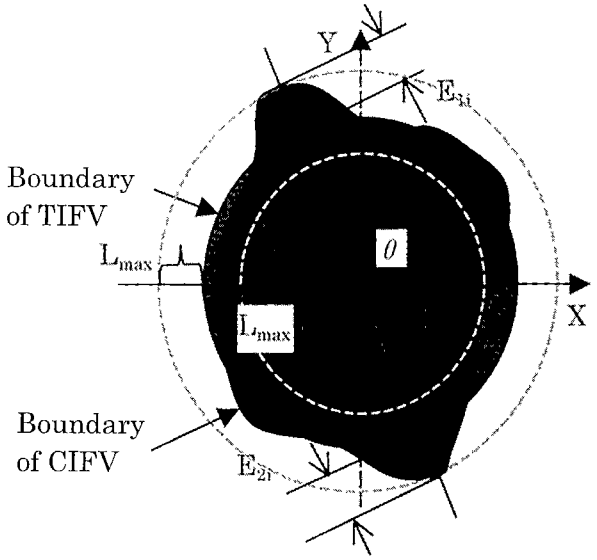

Fig.6(a) The enlarged image of error size between the external edge of CIFV and that of TIFV

Usually these values are calculated based on perimeter, radius or diameter and the coordinates of the center of circle. However, in many cases, the circle may be in bad condition, e.g. the boundary of the circle is not smooth, so that the radius is difficult to be calculated. So we present a more simple method to represent feature values, rather than to calculate the values directly.

Fig.6(a) demonstrates the ring of the enlarged difference between the external edge of CIFV and that of TIFV. By rotating the ring from 0 to 180^0 ($0 \leqq \theta < \pi$) in n steps to calculate the pixel numbers E_{1i} and E_{2i} along the X-axis. Before calculation of the feature values, the dimension was detected approximately by the following limitation.

$$|E_{1i}| < \alpha \times L_{max} \text{ and } |E_{2i}| < \alpha \times L_{max} \qquad 0 < i < n$$

where L_{max} represents the allowed tolerance which is shown in Fig.2(b). α is a coefficient.

If E_{1i} or E_{2i} meet the requirement above, we continue to evaluate the quality by the following algorithms. Otherwise we can determine that this component is bad one directly. Then the feature descriptions can be given by the following equations:

(1) Error sizes The error sizes of the external circle are divided into two parts $E\Omega_{1e}$ and $E\Omega_{2e}$.

$$E\Omega_{1e} = S_t - S_t \cap S_e \text{ or } (\Omega_1 \in \{M(i,j)=a_1\})$$

$$E\Omega_{2e} = S_e - S_t \cap S_e \text{ or } (\Omega_2 \in \{M(i,j)=a_2\}) \quad \text{.....(2)}$$

where S_t and S_e represent the areas (pixel numbers) of the template and the captured images, respectively. The area $E\Omega_{1e}$ refer to the pixel number of concave area and $E\Omega_{2e}$ refer to the pixel number of convex area shown in the Fig.6(a). If the values $E\Omega_{1e}$ and $E\Omega_{2e}$ are zero or near zero, then the measured object in the front view must be a good component. Otherwise the quality must be determined by considering other features.

(2) Circularity(roundness) This value is evaluated by the following equation:

$$\delta_e^2 = \left(\sum_{i=1}^{n}(E_{1i}-e)^2 + \sum_{i=1}^{n}(E_{2i}-e)^2\right)/2n \quad \text{.....(3)}$$

where $e=\left(\sum_{i=1}^{n}E_{1i}+E_{2i}\right)/2n$, and E_{1i} and E_{2i} are the pixel numbers between the edge of CIFV and TIFV. In the case the edge of the captured image is on the outside of the edge of template image, the value of the pixel number is positive, in the opposite case, the pixel number is negative.

(3) Symmetry of the circle The symmetry is evaluated by the equation (4).

$$S_e = \sum_{i=1}^{n} |(E_{1i}-E_{2i})|/n \quad \text{.....(4)}$$

If the value is zero or near zero, this symmetry is in good condition. Fig.6(b) show a situation which circularity is not in good condition. But if the symmetry of circle is good, then this component in front view also can be considered as a good one.

(4) Eccentricity Fig.6(c) shows the eccentric case between the internal and external circles. As described in section **3.2.2** the coordinate $(I_{o'},J_{o'})$ of the center point(O') and (o)$(i_o j_o)$ can be calculated. The distance (O'o) is calculated by the following equation:

$$O'o^2 = (X_{o'} - x_o)^2 + (Y_{o'} - y_o)^2 \quad \text{.....(5)}$$

O'o represents the eccentricity between the two circles. Therefore, there are nine feature parameters for evaluating the quality of front size.

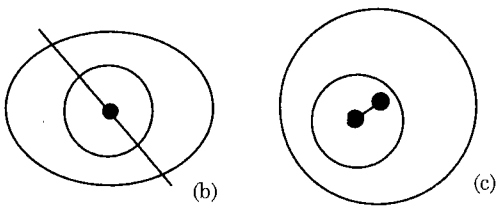

Fig.6(b) a shape of the circle in special case, Fig.6(c) eccentricity between internal and external circles.

As mentioned above the values $E\Omega_{1e}$ and $E\Omega_{2e}$ represent the error size of external circle. δ_e^2 and S_e represent the circularity and the symmetry of the external circle. The other feature values ($E\Omega_{1i}$ $E\Omega_{2i}$, δ_i and S_i) for evaluating the internal circle can be calculated in the same way. We can calculate the limitation of those values to determinate the quality based on the designed tolerance. This problem will be described in Appendix

4.2.2 Feature parameters for the side view In the side view, Fig.7(b) shows an example of matching result between the TISV and CISV. The feature values was calculated only based on the positions of five horizontal scanning lines(1-1',2-2',3-3',4-4',5-5') and two vertical scanning lines (X_1-X_2, X_1'-X_2'). The line positions depend on template image shown in Fig.7(a).

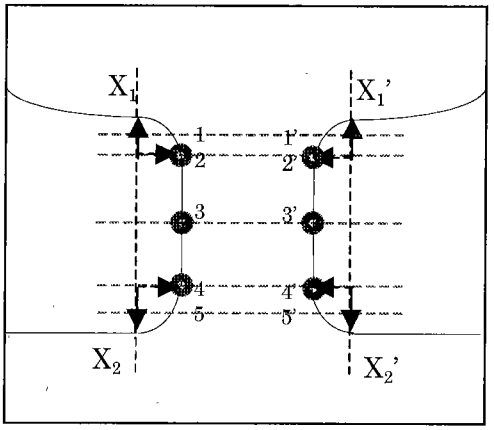

Fig.7(a) The tested position indicated by the dotted lines in TISV for measuring the result shown in Fig.7(b)

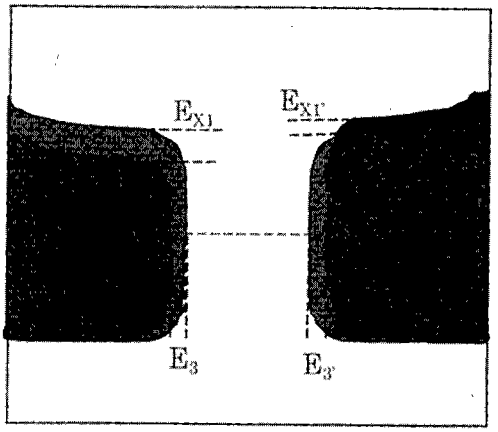

Fig.7(b) The enlarged image of error size between the edge of CISV and that of TISV

In each line, there are two values in the left and the right positions of the hole, which represent the matching result of the difference between CISV and TISV in each line. The pixel numbers of the different sizes are calculated by the following equations:

$$E_i = \sum_{j=0}^{255} P(i,j), \quad E_i' = \sum_{j=255}^{511} P(i,j) \quad \text{.....(6)}$$

$$i \in \{i_1, i_2, i_3, i_4, i_5\}$$

$$E_{xj} = \sum_{i=0}^{255} P(i,j), \quad E_{xj}' = \sum_{i=255}^{511} P(i,j) \quad \text{.....(7)}$$

$$j \in \{j_{x1\text{-}X1'}, j_{x2\text{-}X2'}\}$$

$$\text{where } P(i,j) = \begin{cases} +1, & if \quad M(i,j) = a_1 \\ -1, & if \quad M(i,j) = a_2 \\ +0, & if \; M(i,j) \in \{|a_1 - a_2|, 0\} \end{cases}$$

M(i,j) is the intensity in the matching image as shown in Fig.7(b). As depicted in Fig.7(a), E_i, and E_i' are the pixel numbers of horizontal scanning lines in the left and the right parts, respectively. E_{xj} and E_{xj}' also denote the pixel numbers of vertical scanning lines in the upper and the lower parts.

The following parameters are important feature parameters to evaluate the quality of the component in the side view:

(1) Symmetry between the left and the right parts in CISV. The value (S_s) is calculated by using the following equation.

$$S_s = S/(N_1+2) \quad \text{.....(8)}$$

where $S=(\sum_{p\in\omega_1} |E_p - E_p'|)+|E_{x1}- E_{x1}'|+|E_{x2}- E_{x2}'|$,

$\omega_1 \in \{1,2,3,4,5\}$, N_1 denotes the number of the sets of ω_1.

(2) Similarity (δ_s) between the template (TISV) and the captured images (CISV) The similarity is defined as follows:

$$\delta_s = (\sum_{p\in\omega_2} |e-E_p|)/N_2 \quad \text{.....(9)}$$

where $e=(\sum_{p\in\omega_2} E_p)/N_2$

$\omega_2 \in \{X_1, X_1', X_2, X_2', 2, 4, 2', 4'\}$,

N_2 denotes the number of the sets of ω_1.

(3) Verticality V of the center hole This value V can be obtained by using the following equation:

$$V=|E_2-E_3|+|E_3-E_4|+|E_2-E_4| +|E_2'-E_3'|+|E_3'-E_4'|+|E_2'-E_4'| \quad \text{.....(10)}$$

where V refers to as verticality of the hole . If V equals to 0 or smaller than a limitation value, then this feature of the component is in good condition.

(4) Error size This value E_s is calculated by using the following equation.

$$E_s=(\sum_{p\in\omega_3} |E_p|) \quad \text{.....(11)}$$

$\omega_3 \in \{X_1, X_1', X_2, X_2', 1, 2, 3, 4, 5, 1', 2', 3', 4', 5'\}$

where E_s represents the error size of CISV.

(5) Maximum error

$$M_e = \text{Max}(E_{x1}, E_{x1}', E_{x2}, E_{x2}', E_1, E_2, E_3, E_4, E_5, E_1', E_2', E_3', E_4', E_5')$$

where M_e represents the maximum error among the tested errors.

This five parameters(S_s, δ_s, V, E_s, M_e)are used to evaluate the quality of the pellet component in the side view.

4.3 The structure of neural networks Because the front and the side views reflect the different features of component, so we use two types of neural networks[14] to evaluate the quality in the front and the side views, respectively.

One set of the input values of the networks is error sizes($E\Omega_{e1}$, $E\Omega_{e2}$, $E\Omega_{i1}$, $E\Omega_{i2}$), the circular degrees (δ_e^2, δ_{in}^2), symmetries (S_e and S_i) and eccentricity(oO') for evaluating the quality of the component in the front view. In the same way, the five values (S_s, δ_s, V, E_s, M_e) are used as input parameters for evaluating the quality in the side view.

Here, we apply the back propagation (BP) networks (15)~(17) as a neural networks structure shown in Fig.8 for classifying the quality of the component. We used three layer structure of PB networks which is easier to be analyzed and have an ability of nonlinear separation for our problem.

The neural classifier gives one output value ranging from 1 to 0, which represents the quality is good or not. The neural networks are three layers: 9(input units) – 15(hidden units) –1(output unit) and 5(input units) – 10(hidden units) –1(output unit) for the front and the side views, respectively. The quality of performance of the neural networks is determined by many factors such as the number of the training exemplars and the number of hidden nodes. Here, the estimation of the number of hidden nodes is an important task. If the number of hidden nodes is too small, the network can not remember the training data. For sufficiently large number of hidden nodes, the network can be optimally trained. So the number of hidden nodes depends on the training exemplars. If the problem is complicated, then it needs more training exemplars to be trained.

Of course, some researchers used other methods such as genetic algorithms to determinate the number of hidden nodes based on the training exemplars.

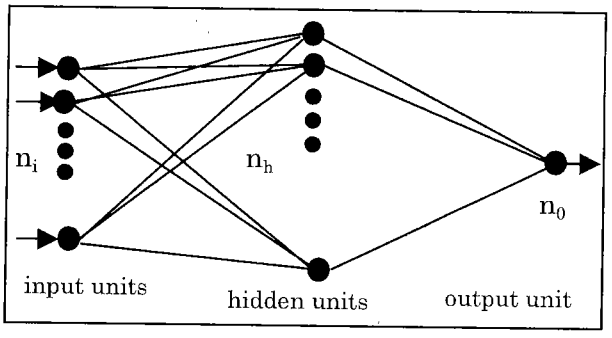

Fig.8 back propagation network structure

Another problem is how to determinate the number of the training exemplars. One is relative to the number of input variables. If the networks need to be developed into arbitrarily complex models of the data, the number of training exemplars must be greater than the number of inputs. Otherwise, the decision boundary is only linear, but not nonlinear. Another one is relative to the worst-case testing error[16] that can be approximately estimated as follows:

Testing error $\approx N_{wg} / N_{tr}$ .....(12)

$N_{wg} = (n_i + n_0) n_h$

where N_{tr} is the number of training exemplars, and N_{wg} is the number of the weights. In addition, n_i ,n_0 and n_h represent number of input, output and hidden layer, separately. From this equation, we can determine the training exemplars approximately.

5. Experimental result and its discussion

5.1 The allowed tolerances of pellet component

Usually, in the different situations of the components, there are different requirements of tolerances. Here the sample PR5-6 was used as an example, which the tolerances were shown in Fig.2(b), to demonstrate our algorithms. Based on the tolerances, we calculate the maximum limitations for each feature parameter. In the meantime, all of the dimensions are changed into the number of pixel. Here, the magnification of lens in microscope is 10. In this case, the interval between two pixels represents 0.732 μ m. According to the tolerances, the maximum limitations of each feature is calculated as follows:(the calculation method is described in Appendix.)

Table 1 Maximum limitation for CIFV

$M_{\Omega e1}$	$M_{\Omega e2}$	M_{Se}	$M_{\delta e}$	$M_{\Omega i1}$	$M_{\Omega i2}$	M_{Si}	$M_{\delta i}$	$M_{O'o}$
4568	4863	13.66	46.66	866	893	4.1	3.07	13.7

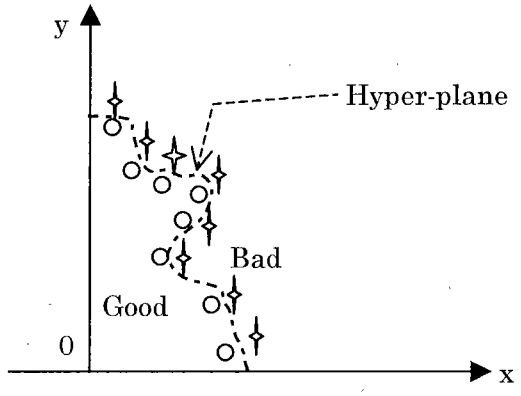

Fig.9 an example of the nonlinear separation

5.2 Training data and the number of exemplars

Because the input vector which contains 9 parameters are difficult to be illustrated by using graph, so we use two dimensions shown in Fig.9 to explain our design for the classification. Supposed the vectors (x,y) are divided into two groups (good and bad groups) by the dotted line which is nonlinear separation. But the curve is very difficult to be described by an equation, therefore, we can select the boundary vectors as marked by circles and stars to train the neural networks. After the neural networks having been trained successfully, that can be used to classify the data into two groups.

In our problem, we also can select the training exemplars to train the neural networks based on the allowed tolerances and the requirements of precision. If the selected exemplars are used to train the NN successfully, the networks can separate the measured component into two groups by a hyper-plane as same as the nonlinear curve as mentioned above. The selection of training examples for classification is described as follows.

(1) If both $E\Omega_{i1}$ and $E\Omega_{i2}$ reach to the maximum limitations, the component is bad one. The limitation has an approximated relationship shown in Fig.10. We use the training exemplars to represent the relationship. The more the exemplars are selected to train, the more precise the network is suitable for the classification.

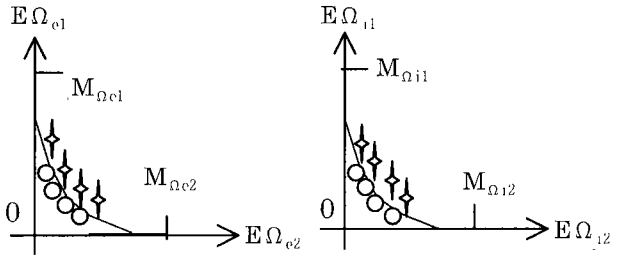

Fig.10 The approximated relationship between the limitations of the error sizes.

(2) The limitation eccentricity O'o has a relationship with other parameters as shown in Fig.11.

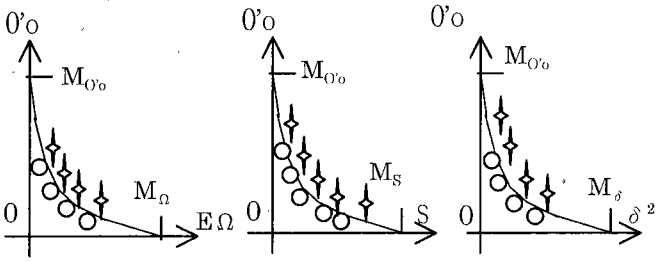

Fig.11 the relation between O'o and the other values

(3) As shown in Fig.6(b), If the symmetry in very good condition (S_e and $S_i = 0$), even other feature values($E\Omega_{e1}$, $E\Omega_{e2}$, δ_e^2) are not in the range of maximum limitation, this component also can be considered as a good one. The new limitations are used as training exemplars which can be gotten from experiments.

(4) Fig.12 shows the relationship between the error sizes E Ω and the roundness(δ_i^2 or δ_e^2).

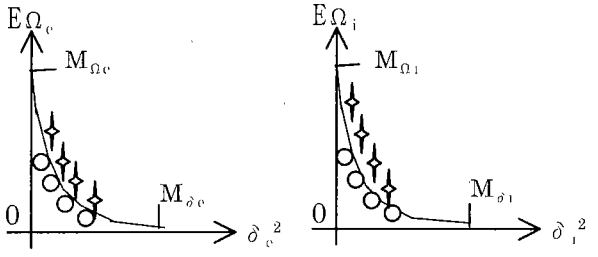

Fig.12 the relationship between error size and roundness

$E\Omega_e$ represents both $E\Omega_{e1}$ and $E\Omega_{e2}$, $E\Omega_i$ represents both $E\Omega_{i1}$ and $E\Omega_{i2}$.

In Figs.10,11 and 12, the upper parts of the curves indicate that the values are larger than the error limitations. Conversely, the lower parts indicate that the values are smaller than the error limitations. Based on those curves, the exemplars are selected.

Other training exemplars are directly gotten from the good and bad components which have been inspected by using the traditional method.

We used 200 training exemplars to train the networks of the front view. In the same way, for the side view, 100 exemplars were used to train.

We have tested the effectiveness of our method by using 70 components (50 pieces are good one, 20 pieces are bad one). The successful rate is up to 100 percent. Because of the errors of the measurement system, The measured data have to be tested for several times. Here, the average of 5 testing values for each measured data was used to calculate the feature values.

Of course, for practical use, 200 training exemplars are not enough, the number also depends on the precision of classification and the structure of NN. According to equation (12), if appropriate training exemplars are used more than 1500, the performance of networks of the front view will be much better.

5.3 Comparison with the traditional methods

The traditional methods[3][4][7][8][9][10] evaluate the precision and accuracy only for a single value such as a length, an angle by using probability and statistics. In the meantime, those traditional methods mentioned above evaluate the quality of a component by using linear determination for each value.

In our method, it is possible for more flexible and more precise way to classify the quality. After the neural networks having been trained by using appropriate training exemplars successfully, the determination is efficient, and the quality of the components can be classified by a non-linear hyper-plane. If there are new designing requirements for evaluating the quality, it will be convenience to add the training exemplars which satisfy the new requirements. By improving the structure of networks and the training exemplars, the ability of determination of the networks can be improved.

6. Conclusion

In this paper, we proposed the global properties of image to determinate the quality of the pellet component based on neural networks by comparing with template image. In addition, we proposed the new algorithms for evaluating the similarity, symmetry and circular degree of the component. The experimental results show the potential efficiency and effectiveness of our method to detect the quality of pellet components. Compared to previous methods, our method has several advantages:

(a) By using template matching, it can avoid the errors risen from locating the measured position [3].

(b) It can inspect the quality in more precise way. It can make nonlinear classification and can cover the situation in more detail by improving the training exemplars.

(c) Our classifier can tell the quality more directly. The processing used neural network is parallel calculation which also has some features of human intelligence.

Of course, we should continue to perfect the structure of neural networks. And using more appropriate data to train the networks and to get the nonlinear hyper-plane of the optimal boundary between good and bad qualities of the tested images, so that it is effective in many situations in practical use. In order to improve the efficiency and effectiveness of this system, we should determine the number of hidden units and the number of training exemplars which are more appropriate to satisfy our system requirement. And continue to research the relationship between the capacity of memory and the number of hidden nodes

(Manuscript received Aug., 23, '99, rivised March, 1, 2000)

References

(1) D. Pohland and M. Redenbacher, "Evaluation of the Automated Hematology Analyzer Sysmex SF-3000™ with Special Regard to Paediatric and Oncology Aspects", Sysmex Journal International, Vol.8, No.1, pp.27-33,1998.

(2) B. S. Pan and Y. T. Wang et al., "Evaluation of Sysmex SF-3000™ Automated Hematology Analyzer", Sysmex Journal International, Vol. 8, No.1, pp. 34-37, 1998.

(3) H. Masada, B. Yichikawa and K. Taniguchi et al., "Dimension Measurement of Pellet Component Which is Used in Automated Hematology Analyzer", Proceeding of the Joint Conference of Hokuriku Chapter of Institutes of Electrical Engineers, Japan, F-19, 1998.

(4) Hitachi Researching Institute, "The General View of Industrial Application of Image Processing " the second part, pp.10-20, 1994.

(5) FLOVEL Corporation: "High Speed Auto-focus AF-2000 guidebook", June,1992.

(6) First Precision Corporation in Japan, "MICRO SCANNER Manual", No.MSOM2 , 1995.

(7) O. Taniguchi and Y. O. Horigome: "Measurement Engineering", Monikita Publish Company, Tokyo, Japan, pp.1-14 ,1997.

(8) N.C. Babford and E. Sakai, "Experimental measurements: precision, error and truth", Maruzen Co. Ltd., Tokyo, 1997

(9) H. Nagazawa "High Precision Engineering", Institute of Industry Investigation, Tokyo, 1993

(10) G. M. Yamaguchi & T. H. Mori, "Measurement Engineering", Kyorituz Publish Company,Tokyo, Japan, pp.142-175 1995

(11) K. Taniguchi, "Image Processing Engineering", Kyorituz Publish Company Tokyo, Japan, pp.126-129,1996

(12) A. D. Bimbo & P. Pala , "Visual Image Retrieval by Elastic Matching of User Sketches" , IEEE Trans. on PAMI , Vol.19, No.2, pp.121-132,1997

(13) D. Weinshall, and M. Werman, "On View likelihood and stability" IEEE transactions on PAMI, Vol.**19**, No. 2, pp.97-108,1997

(14) Kazuhiro kohara and Yukihiro Nakamura, "Modifying Desired Outputs to improve Pattern Recognition by Combining Sub-feature Input Neural Networks", Trans. of IEE of Japan, Vol.117-C, No.6, pp.805-813,1997

(15) B. Nicolao and N. Anastasios, "Artificial Neural Networks: Learning Algorithm, Performance Evaluation and Applications", Kluwer Academic Publishers, Massachusets, USA, pp.87-131, 1993

(16) J. R. Edward, "Neural network data analysis using Simulnet", Springer-Verlag NewYork, Inc, pp.38-40, 1998

(17) Y. H. Pao, "Adaptive Pattern Recognition and Neural Networks ", Addison-Wesley Publish company, Inc. 1989

Appendix

An example for calculation of maximum limitations

Those values are calculated based on the tolerance and the requirements. The following shows an example how to calculate the values. As shown in Fig.2(b), the length of external diameter(D) is $160\,\mu$m and the tolerance(T) is $\pm 10\,\mu$m. The internal diameter(d) is $100\,\mu$m and its tolerance(t) is $\pm 3\,\mu$m. Then the values of external circle R, R_{max}, R_{min} equal to $80\,\mu$m, $85\,\mu$m and $75\,\mu$m, separately. The positions of them are shown in Fig.A. In the same way, the values of internal circle r, r_{max}, r_{min} equal to $50\,\mu$m, $51.5\,\mu$m and $48.5\,\mu$m, separately. The maximum limitations can be calculated as follows:

1. The maximum limitations of error sizes of the area Ω_e in the external circle are calculated as follows.

$$M_{\Omega e1} = \pi \times (R^2 - R_{min}^2)/u^2$$
$$= \pi \times (80^2 - 75^2)/0.732^2 = 4568.8$$
$$M_{\Omega e2} = \pi \times (R_{max} - R)^2/u^2$$
$$= \pi \times (85^2 - 80^2)/0.732^2 = 4863.6$$

where u represents the length of interval between two pixels, $M_{\Omega e1}$ and $M_{\Omega e2}$ represents negative and positive errors, respectively.

2. The maximum limitations of error sizes of area Ω_i in internal circle are calculated as follows.

$$M_{\Omega i1} = \pi \times (r^2 - r_{min}^2)/u^2$$
$$= \pi \times (50^2 - 48.5^2)/0.732^2 = 866.3$$
$$M_{\Omega i2} = \pi \times (r_{max}^2 - r^2)/u^2$$
$$= \pi \times (51.5^2 - 50^2)/0.732^2 = 892.7$$

3. The maximum limitations of symmetries of both external and internal circles are calculated as follows.

$$M_{Se} = (D_{max} - D) \times n/(n \times u) = 10/0.732 = 13.66$$
$$M_{Si} = (d_{max} - d) \times n/(n \times u) = 4.098$$

where the n represents the rotation steps, M_{Sc} and M_{Si} represent the symmetries of the external and internal circles, respectively.

4. The maximum limitations ($M_{\delta e}$ and $M_{\delta i}$) of circularities of both external and internal circles are calculated as follows.

$$M_{\delta e} = \left(\sum_{i=1}^{n}\left(\frac{T}{2} - e\right)^2 + \sum_{i=1}^{n}\left(\frac{T}{2} - e\right)^2\right)/(2n \times u^2)$$
$$M_{\delta e} = (n \times (5-0)^2 + n \times (5-0)^2)/(2n \times 0.732^2)$$
$$= 46.66$$
$$M_{\delta e} = \left(\sum_{i=1}^{n}\left(\frac{t}{2} - e\right)^2 + \sum_{i=1}^{n}\left(\frac{t}{2} - e\right)^2\right)/(2n \times u^2)$$
$$M_{\delta i} = (n \times (1.5)^2 + n \times (1.5)^2)/(2n \times 0.732^2)$$
$$= 3.07$$

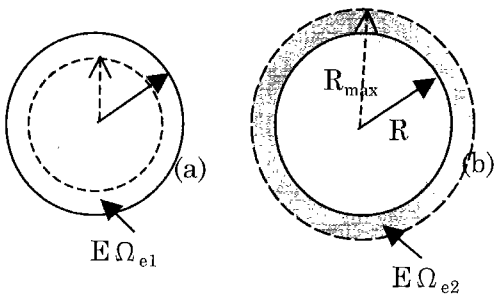

Fig.A The designed tolerance of circle:
(a) negative errors, (b)positive errors

Ningfeng Zeng (non-member)

He has joined Department of Information Science, in Fukui University to pursue doctoral studies since 1998, his current interests include machine learning, reasoning under uncertainty, computer vision and pattern recognition.. IEEE Member

Hiroshi YAMAMOTO (non-member)

He is an executive manager of SYSMEX Corporation, Kobe City, Japan

Toshihiro KONAKA (non-member)

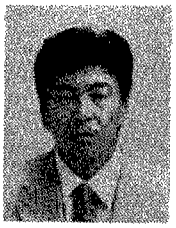

He is an engineer of Department of Manufacturing Technology in SYSMEX Corporation, Kobe City, Japan

Keiji Taniguchi (member) received a BE. Degree in

Electrical Engineering from Kinki University, Osaka, Japan, in 1964 and a Dr. of Eng. degree from Osaka University in 1972, respectively.

He was a Research Associate of Electronics Engineering at Osaka, University from 1964 to 1973, an Associate Professor of Electronics Engineering of Fukui University from 1973 to 1976 and a Professor of Electronics Engineering and Information Engineering at Fukui University from 1976 and 2000. He has been both Honorary Professors of Fukui University and XI'an University of Technology in China. He has published 10 textbooks, and more than 130 papers in technical journals.